Available online at www.sciencedirect.com
SCIENCE DIRECT®
Journal of Nuclear Materials 354 (2006) 123–130
journal of nuclear materials
www.elsevier.com/locate/jnucmat

Strain hardening and long-range internal stress in the localized deformation of irradiated polycrystalline metals

Thak Sang Byun *, Naoyuki Hashimoto

Oak Ridge National Laboratory, Materials Science and Technology Division, 1 Bethel Valley Road, Building 4500S, P.O. Box 2008, MS-6151, Oak Ridge, TN 37831-6151, USA

Received 25 November 2005; accepted 27 February 2006

Abstract

Low-temperature irradiation can significantly harden metallic materials and often results in microscopic strain localization such as dislocation channeling during deformation. In true stress–true strain analyses, however, the strain localization does not significantly affect macroscopic strain-hardening behavior. It was attempted to explain the strain-hardening behavior during strain localization in terms of long-range back stresses. In theoretical modeling the long-range back stress was formulated as a function of the number of residual pileup dislocations at a grain boundary and the number of localized bands formed in a grain. The strain-hardening rates in channel deformation were calculated for ten face-centered cubic (fcc) and body-centered cubic (bcc) metals. A few residual dislocations in each channel could account for the strain-hardening rates as high as those for uniform deformation. It was also shown that the strain-hardening behavior predicted by the long-range back stress model resembled the empirical strain-hardening behaviors, which result from both localized and non-localized deformations. The predicted plastic instability stress was comparable to the tensile test data.

1. Introduction

Small defect clusters produced by low temperature irradiation can result in dislocation channeling during deformation. In the channeling process the dislocation glide, confined in a narrow bands (~0.1 μm wide), removes defects around the glide planes, leaving a defect-free band. In previous studies [1–8] the softening effect due to the defect clearance and excessive stress concentration at the channel tip have been emphasized to explain the degradation of mechanical properties such as the loss of uniform ductility and the decrease of strain-hardening rate. A large yield drop or a prompt plastic instability after irradiation have been believed to correspond to the initiation of channeling, and indeed many bcc and hexagonal-closed packed (hcp) metals showed the coincidence of channeling and prompt necking at yield [8–11]. In many fcc metals, however, the channel deformation occurred well before the initiation of necking deformation [12], along with a high positive strain-hardening rate [13–15].

Although the decrease of hardening capability with radiation dose is evident in engineering

* Corresponding author. Tel.: +1 865 576 7738; fax: +1 865 574 0641.
E-mail address: byunts@ornl.gov (T.S. Byun).

0022-3115/$ - see front matter © 2006 Elsevier B.V. All rights reserved.
doi:10.1016/j.jnucmat.2006.02.099

stress–strain curves, a few recent studies [13–18] indicate that the strain localization may not significantly affect the strain-hardening rate at a given true stress. A good example for this is neutron-irradiated 316 austenitic stainless steel: although the slope of engineering stress–strain curve decreases with dose at a given elongation and a yield drop become visible for doses above 0.01 dpa [14], Fig. 1, the true strain-hardening rate at a given true stress for irradiated stainless steel is comparable or greater than that of the unirradiated material, Fig. 2. (A small amount of martensite formation is believed to be responsible for the slightly increased strain-hardening rate after irradiation.) It was also shown that the strain-hardening rate during necking was always positive until failure occurred [13,15,16]. The microscopic deformation mode changed from dislocation tangles (cell formation) to channeling at about 0.1 dpa [9]. These results could be explained by a rapid recovery of strain-hardening rate in channels after initial softening due to defect removal. Since few tangled dislocations are found in the channels, it is believed that the positive strain-hardening rate is primarily attributed to long-range stresses [1–3,14,15]. Estimation of the long-range back stress in channeling process has seldom been attempted for polycrystalline metals [3].

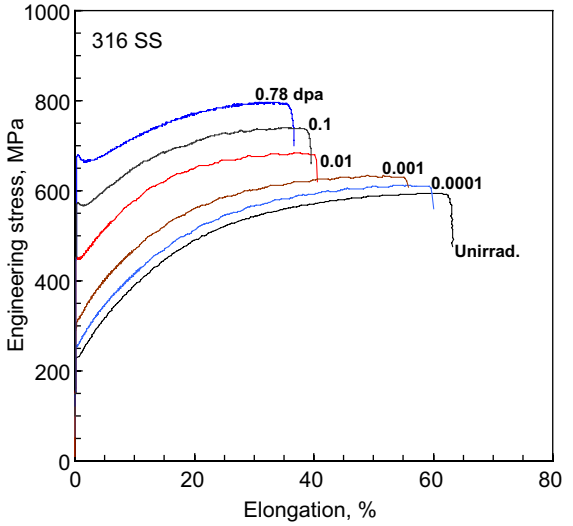

Fig. 1. Engineering stress–strain curves for 316 stainless steel. The specimen deformed by channeling at 0.78 dpa.

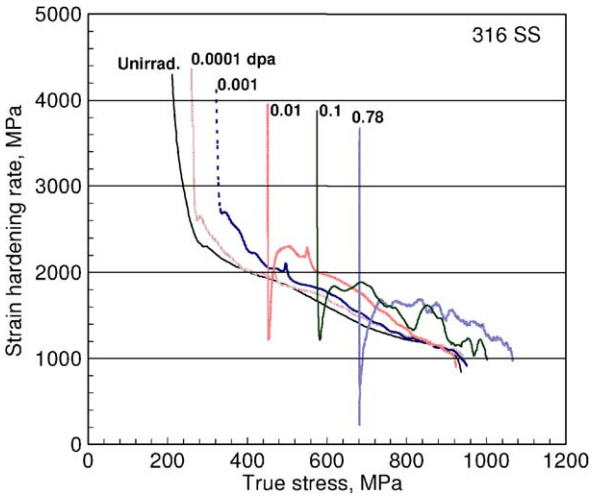

Fig. 2. Kocks–Mecking plots (strain-hardening rate versus true stress curves) for 316 stainless steel before and after irradiation.

In this paper, a simplified model of the channeling process is proposed to explain the strain-hardening characteristics of localized deformation in polycrystalline metals. The initial dislocation pile-up against a grain boundary in the channeling process is modeled to calculate the number of glide dislocations. The increase of plastic strain is assumed to result from the multiplication of parallel channels. The strain-hardening rate due to the long-range back stress exerted by the residual dislocations at the grain boundary was calculated and compared with experimental strain-hardening data. Calculations indicate that that, after multiple channels formed in a grain, a few dislocations per channel can introduce large back stress hardening over the entire grain.

2. Modeling and calculation

2.1. Channeling process and calculation of long-range back stress

A typical channel is generated by the glide of hundreds to thousands of dislocations on adjacent slip planes [1–7]. Observations on surface slip band formation suggest that channels are formed in a short period of 1–2 μs [3]. It is unlikely that the dislocations are generated and glide to the specimen surface one-by-one, even under static loading. Especially in polycrystalline specimens, single dislocation may not be able to cut through grain boundaries. Further, the interaction of a channel with a boundary or other channel shows that the shear strain within a channel is evenly distributed [2]. These can be evidence for a rapid, simultaneous glide of pileup dislocations, which may be produced in the form of a two-dimensional array on hundreds of slip

planes. Dislocations in the pileup may glide nearly simultaneously during a rapid channel growth.

If defect-free channels are observed in a deformed grain, it indicates that the pileups formed at grain boundaries have already moved into adjacent grains. For a channel, the total shear displacement transferred by glide of N_C dislocations with Burgers vector $\vec{b}$ is given by $N_C\vec{b}$. Since this vector displacement cannot be completely transferred to the adjoining grain by glide to the same direction unless the orientations of the two grains are perfectly identical, some amount of the displacement must remain at the grain boundary in the form of a small dislocation pileup. The glide of hundreds to thousands of dislocations in a channel is necessary to produce typical shear displacements of 0.1 μm [1–3,9–11].

In the case that the orientations of two adjoining grains are so different that a geometrically compatible slip system does not exist in the two grains, the propagation of the initial channel and formation of additional channels cannot occur when the applied stress is less than the total resistance stress, including back stress from the dislocation pileup against a grain boundary [10,12]; otherwise a crack should form at the grain boundary to relax the high local stress in front of the pileup. Since in a typical grain in annealed materials the back stress from a pileup of a few hundred dislocations can easily exceed the flow stress level of the material, channel deformation might occur more easily in the grains whose adjacent grains have similar orientations. Thus, when well-developed channels are observed in a grain, the adjacent grain to which shear displacement has been transferred, or from which channels have been propagated, should have geometrically compatible slip system, and consequently the number of residual dislocations at the grain boundary, or unrelaxed displacement vector, should be small. Based on this, a highly simplified model for the channeled grain is presented in Fig. 3, where the grains include multiple channels and each channel retains a few residual dislocations at grain boundary.

If a small pileup of N_R residual edge dislocations exist in the ith channel at the boundary of grains A and B and dislocations are being generated at a source, the back stress exerted to the source from these residual dislocations at a channel can be calculated by [19,20]

$$\tau_B^i = \frac{\mu N_R b}{2\pi(1-\nu)} \frac{L(L^2-h_i^2)}{(L^2+h_i^2)^2}, \tag{1}$$

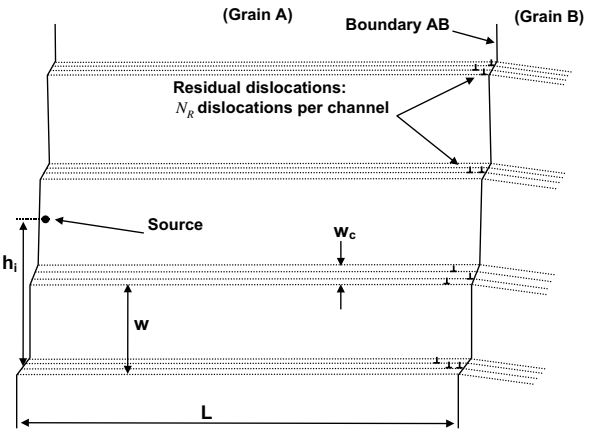

Fig. 3. Schematic of channeled microstructure with small residual dislocation pileups against grain boundary.

where L and h_i are defined as the grain size and vertical distance between the source and the residual pileup, respectively (see Fig. 3). Note that the back stress will be higher approximately by a factor of $(1-\nu)$ if all the pileup dislocations are pure screw. Also, when tangled or randomly distributed dislocations are accumulated at the grain boundary, the vector summation of their Burgers vectors should be considered in the evaluation of long range stress. Assuming that there are N_G channels in the grain, the total back stress is calculated by summation of back-stress components:

$$\tau_B = \frac{\mu N_R b}{2\pi(1-\nu)} \sum_{i=1}^{N_G} \frac{L(L^2-h_i^2)}{(L^2+h_i^2)^2}. \tag{2}$$

Assuming that strain hardening during pure channeling process is mainly due to the back stress, the applied stress τ_A, or the flow stress of a material, should be expressed by

$$\tau_A = \tau_Y + \tau_B, \tag{3}$$

where τ_Y is the yield stress; the lower yield stress should be used if there is yield drop. Then the strain hardening rate is calculated by

$$\frac{d\tau_A}{d\gamma} = \frac{d\tau_B}{d\gamma}, \tag{4}$$

or in principal stress (σ) and principal strain (ε) terms,

$$\frac{d\sigma}{d\varepsilon} = M^2 \frac{d\tau_B}{d\gamma}, \tag{5}$$

where M is the average value of Taylor factor: 2.75 for equiaxed bcc metals and 3.07 for fcc metals [19].

To evaluate these equations, the number of residual dislocations N_R and the number of channels in a grain N_G need to be estimated. First, the value of N_R is calculated by assuming that in the channeling process dislocation glide into grain B continues to occur until the forward stress at grain B, in front of a residual dislocation pileup (see Fig. 3), becomes smaller than the total resistance stress including the bowing stress of a dislocation at grain B. We also assume that the channels propagate through the grain boundary only if closely oriented slip systems exist in grains A and B. When a dislocation propagates from grain A into grain B, the forward stress at grain B from the residual dislocations piled up at the grain boundary is derived from Eq. (1) by setting $L = \rho$ and $h_i = 0$,

$$\tau_P = \frac{\mu N_R b}{2\pi(1-\nu)\rho}. \tag{6}$$

It is assumed that the dislocation that has passed through the grain boundary or is newly-generated at a source, which exists next to the boundary always starts to glide by forming and expanding a circular portion. The stress for bow-out of a dislocation with curvature ρ is given by [19]

$$\tau_R = \frac{\mu b}{2\rho}. \tag{7}$$

The vector components of glide plane and direction for gliding dislocations have to be changed in the transfer of shear displacement through a grain boundary. Then, a stress balance equation for the last dislocation being transferred into grain B can be formed as

$$\tau_A + \frac{\mu N_R b}{2\pi(1-\nu)\rho} = \tau_0 + \frac{\mu b}{2\rho}, \tag{8}$$

where the term τ_0 is the resistance stress excluding the bowing stress. Rearranging for N_R,

$$N_R = \pi(1-\nu) - \frac{2\pi(1-\upsilon)(\tau_A - \tau_0)\rho}{\mu b}. \tag{9}$$

Assuming that the curvature of an expanding dislocation is very small, the second term in the right side of this equation is neglected in the calculation.

To evaluate Eq. (2), we also need to calculate the number of channels per grain N_G. Here N_G is calculated by dividing total shear γL by channel shear $N_C b$. The number of dislocations piled up at a grain boundary is calculated from the first channel formation, where all of the glide dislocations generated from a source are piled up against the grain boundary before the channel propagates to the next grain. If we assume that radiation-induced defects in a channel are completely removed by N_C glides, the local yield stress will be reduced to τ_0 within the channel. An upper limit on the number of channeling dislocations, N_C, can be obtained when the operation of a dislocation source is stopped by the back stress from pileup dislocations. Using an approximated expression for the long-range back stress and the condition $\tau_A = \tau_Y$ for the first channel, the stress balance for a dislocation at the source in grain A is given by

$$\tau_Y = \tau_0 + \frac{N_C \mu b}{2\pi(1-\upsilon)L}. \tag{10}$$

This can be rewritten for the channel shear $N_C b$

$$N_C b = \frac{2\pi(1-\upsilon)(\tau_Y - \tau_0)L}{\mu}. \tag{11}$$

Then, we can calculate N_G in the channel by

$$N_G = \frac{L}{w} = \frac{\gamma L}{N_C b} \quad \text{with } w\gamma = N_C b, \tag{12}$$

where w is the spacing between channels.

2.2. Property data for calculation

This paper presents calculated back stress hardening data for six bcc metals: A533B steel, V, Nb, Fe, Mo, and Ta and four fcc metals: 316 stainless steel, Al, Cu, and Ni. The A533B steel was in a quenched and tempered condition and the others are in annealed conditions. Details of the heat treatment conditions and chemical compositions are given in Refs. [9–11,15]. A custom-designed miniature sheet tensile specimen with gage section dimensions of 1.5 mm wide, 0.25 mm thick, and 8 mm long was used. Tensile tests were conducted at room temperature at a nominal crosshead speed of 0.008 mm s^{-1}, which gave a strain rate of 10^{-3} s^{-1}.

Table 1 lists the strength data and basic physical properties for the unirradiated materials, which were needed for calculation. The data include yield stress (YS), ultimate tensile strength (UTS), plastic instability stress (PIS), Young's modulus (E), shear modulus (μ), Poisson ratio (ν), Burgers vector size (b), and grain size (L). The true plastic uniform strain ε_U^P was calculated from the uniform elongation UE (in %) using the definition of logarithmic strain $\varepsilon_U^P = \ln(1 + \mathrm{UE}/100)$. Then the UTS was converted to the true stress unit or so-called the plastic instability stress (PIS) using the expression $\mathrm{PIS} = \mathrm{UTS} \times \exp(\varepsilon_U^P)$ [14,15].

Table 1
Strength data and physical parameters for pure metals and alloys before irradiation

Materials	Crystal	YS (MPa)	UTS (MPa)	PIS (MPa)	M	b (nm)	E (GPa)	μ (GPa)	ν	L (μm)
A533B	BCC	504	630	715	2.75	0.2482	208.2	80.7	0.291	30[a]
Fe	BCC	213	241	304	2.75	0.2482	208.2	80.7	0.291	35
V	BCC	304	334	397	2.75	0.2622	127.6	46.7	0.365	30
Nb	BCC	239	303	368	2.75	0.2853	104.9	37.5	0.397	30
Mo	BCC	473	550	630	2.75	0.2725	324.8	125.6	0.293	60
Ta	BCC	271	343	283	2.75	0.2856	185.7	69.2	0.342	60[a]
316SS	FCC	205	515	901	3.07	0.2525	215.3	83.9	0.283	10[b]
Al	FCC	29	75	100	3.07	0.2864	70.6	26.2	0.345	30[a]
Cu	FCC	39	215	300	3.07	0.2557	129.8	48.3	0.343	18
Ni	FCC	59	317	541	3.07	0.2487	207.0	76.0	0.312	30

[a] Typical grain size in annealed condition.
[b] Approximate effective grain size considering anneal twins (the austenite grain boundary of annealed 316 stainless steel was 30–67 μm).

3. Results and discussion

Fig. 4 displays the calculated strain-hardening rates as functions of yield stress. The strain-hardening rates were calculated for the condition that strain was produced by channeling processes only. Since the metals may not deform in a localized manner at low yield stresses, the low yield stress portion of each curve should be considered invalid; especially the room temperature deformation after irradiation to low doses (<~0.01 dpa), which is always uniform in the whole strain range. Also, other possible hardening mechanisms such as the intersections between channels, and the formation of stacking faults and twins were not taken into account in the present calculation. As seen in Fig. 4, however, the calculated strain-hardening rate decreases with increasing yield stress, and the yield stress dependences of those hardening rates resemble those of Kocks–Mecking plots or strain hardening rate versus stress plots [21,22]. This result indicates that both the uniform and localized deformations produce similar strain-hardening behaviors, and therefore the change in strain-hardening rate should not be used as single evidence of channeling.

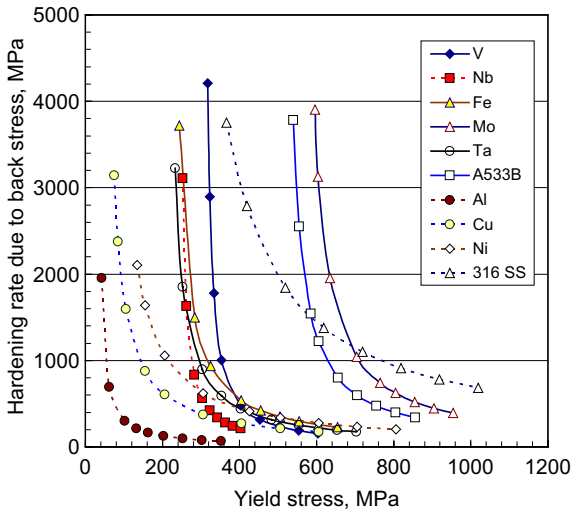

Fig. 4. Calculated strain-hardening rate as function of yield stress for bcc and fcc metals. Only channel deformation was considered in the calculation; the results are not be valid for low yield stress cases where channeling does not occur although the predicted strain-hardening rate are similar to the experimental data.

Since the long-range stress hardening is caused by the dislocations which piled up at grain boundary, the number of those residual dislocations is a key parameter in the calculation. Table 2 includes the calculated number of residual dislocations, along with other dislocation number data. (Eqs. (9)–(11) were used for the calculation of the dislocation numbers.) Only about 2 dislocations per channel are necessary to produce high strain-hardening rates as high as PIS. Those residual dislocations are a small portion of the glide dislocations necessary to form a channel. In the channel deformation at PIS, for example, the number of gliding dislocations per channel, N_C, are in the range 400–900. This indicates that only small portion, 0.25–0.5%, of the glide dislocations remains at grain boundary and produces back stress to dislocation sources. However, it is worth noting that the total number of residual dislocations will keep increasing as more channels are formed. To accommodate a 5% strain in a grain with N_C glide dislocations; for example, some 13 channels are necessary for 316 stainless steel and 52 channels for molybdenum. These correspond to

Table 2
Examples of dislocation numbers for channel deformation

Materials	Crystal	YS (=Predicted PIS) (MPa)	N_C	N_G	N_R	$N_G \times N_R/L$ (dislocations/μm)
A533B	BCC	682	432	41	2.2	3.0
Fe	BCC	450	671	30	2.2	1.9
V	BCC	420	412	41	2.0	2.7
Nb	BCC	343	402	38	1.9	2.4
Mo	BCC	760	594	52	2.2	1.9
Ta	BCC	420	776	40	2.1	1.4
316SS	FCC	860	453	13	2.3	3.0
Al	FCC	165	729	21	2.1	1.5
Cu	FCC	340	655	17	2.1	2.0
Ni	FCC	425	818	21	2.2	1.5

Note: N_C-numbers of glide dislocations per channel when YS = PIS; N_R-residual dislocations per channel; N_G-number of channels in a grain at 5% strain.

3 and 1.9 residual dislocations per μm in stainless steel and molybdenum, respectively. The density of residual dislocations at a grain boundary is highest in the commercial steels, austenitic stainless steel and A533B steel, than in pure metals. This reflects higher strain-hardening rates in these steels.

Fig. 5 presents the true stress–true strain curves predicted for necking deformation in 10 polycrystalline metals, in which N_C was fixed at the values listed in Table 2. Also, the yield stress was set at PIS since it was reasonable to assume that most irradiated materials would experience channel deformation when they were hardened by irradiation to their PIS values, and again the deformation was assumed to occur by channel formation only. Except for early portions of the curves, where slightly higher strain-hardening rate are calculated, the true stress–true strain curves are linear; strain-hardening rates are constant in the strain ranges considered. This linear hardening behavior agrees with several experimental results that show a linear hardening during necking [16,23,24]. Among the fcc metals Al, Ni, and Cu are relatively low strength materials, while the 316 stainless steel is the highest strength material. Its true flow stress is the highest among all metals considered here. This unique behavior is considered as a result of low stacking fault energy (<20 mJ/m^2), which induces annealing twins and prohibits cross slips. In the present calculation an effective grain size of 10 μm was used for 316 stainless steel to consider the effect of annealing twins [19]. Due to the low stacking fault energy, deformation twins and large stacking faults, which can act as boundaries, are also formed during deformation. Very similar back-stress hardening behaviors are predicted for both channeling and mechanical twinning mechanisms. The effect of twin formation on strain-hardening behavior will be discussed in detail in a separate report. Fig. 5 also shows that the bcc metals are usually stronger than the fcc metals excluding the 316 stainless steel.

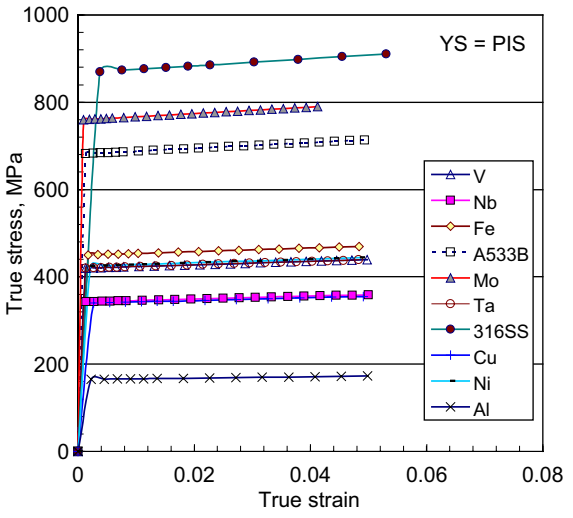

Fig. 5. True stress–true strain curves predicted for necking deformation. Yield stress is set at the onset of plastic instability (YS = PIS), and the deformation is assumed to occur by channel formation only.

Fig. 6 compares the predicted and experimental plastic instability stress values for the metals. Al, Ta, and Fe are among those showing highest discrepancies in percent. The present model overestimates the PIS values for those metals, while the predicted PIS values for the other metals agree well with the empirical values from tensile test data. Figs. 5 and 6 indicate that the strain hardening behavior calculated by considering only long-range back stress can account for empirical strain-harden-

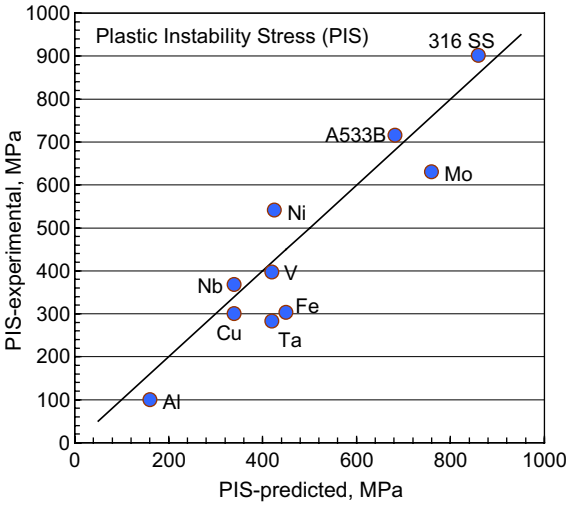

Fig. 6. Comparison of predicted and experimental plastic instability stresses.

ing behavior. Although the present model is not valid for the unirradiated materials that do not exhibit channeling, the calculation assuming channel deformation only produced similar strain-hardening behavior as that of the uniform deformation.

Irradiation hardening often causes a significant change in deformation mechanisms from random dislocation glides to dislocation channeling or twinning. Especially in austenitic stainless steels, the deformation after low temperature neutron irradiation can produce dislocation tangles, stacking faults/twins, and defect-cleared channels [9,25,26]. Regardless of this variety of microstructures, the strain-hardening behavior is comparable for the localized deformation conditions, as seen in Fig. 2 [14]. To explain the dose and mechanism independence of strain-hardening behavior, the authors have suggested two possible reasons [14]: (1) Similar true strain-hardening behaviors can be produced by the channel deformation in irradiated materials and by the uniform deformation in unirradiated materials. (2) Deformations in irradiated materials and in heavily-deformed unirradiated materials are both equally localized.

The present theoretical approach confirms that at least the first suggestion can be correct: Comparing the predicted data in Figs. 5 and 6 and experimental data in Figs. 1 and 2 indicate that the strain-hardening rates due to the long-range back stress in channel deformation can be as high as those in the uniform deformation involving tangled dislocations. A significant drop of local shear stress in the channel should occur because of the defect clearing in the early stages of channel formation; however, the local stress should return quickly to a stress level as high as those in adjacent regions as the back stress builds up [2,3,14]. The conditions for plastic instability imply that, as long as the channel formation spreads to adjacent regions, the local strain-hardening rate must be positive. This is because a negative local strain hardening will cause immediate shear failure without forming a diffused necking which can give rise to a large necking ductility. No negative slope in the true stress–true strain curve has been calculated for the necking deformation after significant irradiation [14–16]. Some of the dislocations generated during channel formation may form pileups against strong obstacles, such as grain boundaries, without being transferred across the boundaries, and the back stress due to the dislocation pileups might stop further source operation and slip in the channel [3,14]. The unresolved displacement component should be accommodated in a form of an unresolved strain component, like dislocation pileups and elastic strains at grain boundaries.

There is also supporting evidence for the second suggestion. Localized (channeled) deformation has been reported for pre-strained pure metals [6,16,27,28]. If the random dislocation glides and localized dislocation glides can harden metallic materials to a similar degree through short-range and long-range stress hardening mechanisms, respectively, both suggestions can be correct, and the influence of deformation mechanisms on strain-hardening rate should not be significant in irradiated materials.

4. Conclusions

(1) A theoretical model was proposed to describe the strain-hardening behavior in strain localization in terms of long-range back stress only. The strain-hardening rate due to the long-range back stress was calculated by summation of shear stress components from the residual pileup dislocations in localized bands.

(2) In 316 stainless steel the strain-hardening behavior predicted by the long-range back stress model was similar to empirical strain-hardening behavior. Further, the predicted plastic instability stress was comparable to the experimental data in all polycrystalline metals examined in this study.

(3) The theory states that only small portion of glide dislocations in a channel, about 2 dislocations per channel, remain against the grain boundary, raising long-range stress. Such a small number of residual dislocations can produce high strain-hardening rate which is comparable to or exceeds the empirical strain-hardening rates.

Acknowledgments

This research was sponsored by US Department of Energy, Office of Fusion Energy Sciences, under Contract DE-AC05-00OR22725 with UT-Battelle, LLC. The authors would like to express special thanks to Drs S.J. Zinkle, J.T. Busby, and Y.N. Osestkiy for their technical reviews and thoughtful comments.

References

[1] J.V. Sharp, Acta Metal. 22 (1974) 449.
[2] J.V. Sharp, Philos. Mag. 16 (1967) 77.
[3] M.J. Makin, J.V. Sharp, Phys. Stat. Sol. 9 (1965) 109.
[4] R.P. Tucker, M.S. Wechsler, S.M. Ohr, J. Appl. Phys. 40 (1969) 400.
[5] M.S. Wechsler, The Inhomogeneity of Plastic Deformation, American Society for Metals, Metals Park, Ohio, 1971, Chapter 2.
[6] A. Luft, Prog. Mater. Sci. 35 (1991) 97.
[7] T.H. Blewitt, R.R. Coltman, R.E. Jamison, J.K. Redman, J. Nucl. Mater. 2 (1960) 277.
[8] K. Farrell, T.S. Byun, J. Nucl. Mater. 296 (2001) 129.
[9] K. Farrell, T.S. Byun, N. Hashimoto, J. Nucl. Mater. 335 (2004) 471.
[10] N. Hashimoto, T.S. Byun, K. Farrell, S.J. Zinkle, J. Nucl. Mater. 336 (2005) 225.
[11] N. Hashimoto, T.S. Byun, K. Farrell, J. Nucl. Mater. 329 (2004) 947.
[12] D.J. Edwards, B.N. Singh, J.B. Bilde-Sørensen, J. Nucl. Mater. 342 (2005) 164.
[13] T.S. Byun, K. Farrell, E.H. Lee, L.K. Mansur, S.A. Maloy, M.R. James, W.R. Johnson, J. Nucl. Mater. 303 (2002) 34.
[14] T.S. Byun, K. Farrell, Acta Mater. 52 (2004) 1597.
[15] T.S. Byun, K. Farrell, J. Nucl. Mater. 326 (2004) 86.
[16] E.V. Van Osch, M.I. DeVries, J. Nucl. Mater. 271&272 (1991) 162.
[17] I.L. Mogford IL, D.J. Hull, Iron Steel Inst. 201 (1963) 55.
[18] S.M. Ohr, Scripta Metall. 2 (1968) 213.
[19] M.A. Meyers, K.K. Chawla, Mechanical Behavior of Materials, Prentice-Hall, Inc., 1998.
[20] J.P. Hirth, J. Lothe, Theory of Dislocations, McGraw-Hill Book Company, 1968.
[21] U.F. Kocks, H. Mecking, Prog. Mater. Sci. 48 (2003) 171.
[22] W. Pantleon, Mater. Sci. Forum 482 (2005) 155.
[23] T.S. Byun, N. Hashimoto, K. Farrell, Acta Mater. 52 (2004) 3889.
[24] T.S. Byun, N. Hashimoto, K. Farrell, J. Nucl. Mater. 351 (2006) 303.
[25] J.I. Cole, S.M. Bruemmer, J. Nucl. Mater. 225 (1995) 53.
[26] T.S. Byun, Acta Mater. 51 (2003) 3063.
[27] B. Brenner, A. Luft, Mater. Sci. Eng. 52 (1982) 229.
[28] J.V. Sharp, M.J. Makin, Can. J. Phys. 45 (1967) 519.